Antiviral Research 192 (2021) 105105

Contents lists available at ScienceDirect

Antiviral Research

journal homepage: www.elsevier.com/locate/antiviral

Research paper

An antibody engineering platform using amino acid networks: A case study in development of antiviral therapeutics

Debbie Ching Ping Lee [a,1], Rahul Raman [b,1], Nahdiyah Abdul Ghafar [a], Yadunanda Budigi [a,*]

[a] Tychan Pte Ltd, 1 Research Link, 117604, Singapore
[b] Department of Biological Engineering, And Koch Institute for Integrative Cancer Research, Massachusetts Institute of Technology, Cambridge, MA, USA

ARTICLE INFO

Keywords:
Antibody engineering
Antiviral therapeutics
Computational design
Zika Disease
Flavivirus
Development of antibody therapeutics
Antibody Platforms

ABSTRACT

We present here a case study of an antibody-engineering platform that selects, modifies, and assembles antibody parts to construct novel antibodies. A salient feature of this platform includes the role of amino acid networks in optimizing framework regions (FRs) and complementarity determining regions (CDRs) to engineer new antibodies with desired structure-function relationships. The details of this approach are described in the context of its utility in engineering ZAb_FLEP, a potent anti-Zika virus antibody. ZAb_FLEP comprises of distinct parts, including heavy chain and light chain FRs and CDRs, with engineered features such as loop lengths and optimal epitope-paratope contacts. We demonstrate, with different test antibodies derived from different FR-CDR combinations, that despite these test antibodies sharing high overall sequence similarity, they yield diverse functional readouts. Furthermore, we show that strategies relying on one dimensional sequence similarity-based analyses of antibodies miss important structural nuances of the FR-CDR relationship, which is effectively addressed by the amino acid networks approach of this platform.

1. Introduction

The discovery and engineering of antibodies as therapeutic agents has undergone a rapid evolution, fueled by the need to shorten the timeline for clinical development especially in the context of rapidly spreading infectious disease outbreaks such as COVID-19 (Lu et al., 2020). In this regard, *in silico* or computational methods (Adolf-Bryfogle et al., 2018; Baran et al., 2017; Entzminger et al., 2017; Poosarla et al., 2017) have complemented *in vitro* and *in vivo* antibody discovery methods (Hu et al., 2015; Scheid et al., 2009) to engineer antibodies with improved binding affinity and other desirable physiochemical properties. These *in silico* tools mostly use molecular docking to identify complementary antigen-antibody binding modes (if the structure of antigen-antibody complex is unknown) and physics-based energy functions to redesign the paratope (Baran et al., 2017; Pantazes and Maranas, 2010).

Development of methods and tools for this antibody engineering platform started with solving a challenging problem of redesigning 4E11, a broad-spectrum anti-Dengue virus (DENV) antibody that neutralized Dengue serotypes DENV-1, DENV-2 and DENV-3, to also neutralize DENV-4 (Tharakaraman et al., 2013). The challenge posed by this problem was two-fold: (1) the structure of 4E11 or its complex with the target epitope was not solved at the time and (2) the redesign effort required simultaneously solving for multiple epitope-paratope interactions to confer binding selectivity to DENV-4 while retaining its existing neutralization properties to DENVs −1, −2 and −3. Several key metrics were developed to solve this problem by mining structural databases of antibody-antigen complexes. These metrics included amino acid interface fitness (AIF) that computed pairwise propensity of amino acids at antigen-antibody interfaces and a standardized epitope-paratope interface index (ZEPII), which computed a score for a given interface calculated based on AIF. By employing a multivariate logic regression (MLR) method that was trained to discriminate native poses of antibody-antigen complexes from decoys, the pose of the 4E11 antibody engaging with its target epitope was accurately predicted and later verified by X-ray crystallography (Cockburn et al., 2012). Using this predicted pose, mutations were engineered on 4E11 to enhance binding affinity of the engineered antibody, referred to as 4E5A, by more than 450-fold compared to 4E11 while retaining 4E11's binding affinity to DENV-1, -2 and -3 serotypes (Tharakaraman et al., 2013).

* Corresponding author.
E-mail address: ybudigi@tychanltd.com (Y. Budigi).
[1] Equal contribution

https://doi.org/10.1016/j.antiviral.2021.105105
Received 13 March 2021; Received in revised form 27 May 2021; Accepted 28 May 2021
Available online 8 June 2021

These tools were expanded through the incorporation of network-based analysis using graph theory approaches (Soundararajan et al., 2011). Both short-range and long-range interactions between non-bonded residues at the epitope-paratope interface were represented as two-dimensional maps (epitope paratope connectivity network or EPCN) and each residue was scored based on its connectivity to other residues in this interface. This network representation permitted detailed investigation of the impact of amino acid changes such as mutations, residue deletions and residue insertions in altering the associated networks. This approach was a significant departure from just viewing amino acid changes as conservative and non-conservative changes respectively, as even conservative substitutions substantially impacted the connectivity of the residues in the network. Using this network-based approach, the 4E5A antibody was further redesigned by introducing two mutations in the heavy chain CDR1 (HCDR1), which included a single residue deletion, that improved the EPCN, enhanced its affinity to all DENV serotypes, and made it clinically developable as a potent pan-DENV therapeutic (Robinson et al., 2015). The overall affinity gain of the engineered antibody was greater than 13,000-fold for DENV-4 (Viswanathan et al., 2015), which ranks amongst the largest affinity enhancement reported by *in silico* antibody affinity enhancement studies (Adolf-Bryfogle et al., 2018; Clark et al., 2006; Farady et al., 2009; Lippow et al., 2007; Marvin and Lowman, 2003).

These tools, initially developed for redesigning antibodies, were used to develop a platform to engineer new antibodies. This antibody-engineering platform enables selection, modification, and assembly of parts (analogous to building blocks or Lego blocks assembly), which comprise of distinct heavy and light chain framework regions (FRs) and complementarity determining regions (CDRs). A key aspect of assembling and engineering the antibody parts involved mining available antibody sequence and structural information to optimally engage with the target epitope surface. The process is an iterative cycle of designing and generating antibodies engineered from different parts followed by experimental screening of these designs for desired properties. The metrics used in the selection and the modifications of parts (including feedback from the experimental screening) include AIF, ZEPII, EPCN and MLR methods.

The Zika outbreak of 2015–2016 highlighted the urgent need for therapeutic options. The antibody-engineering platform was deployed to rapidly engineer a neutralizing antibody to target an epitope that was specific to the Zika Virus and posed minimum risk of escape mutations. The functional attributes of the resulting antibody, ZAb_FLEP, have been described in some detail previously in a *Cell Host and Microbe* paper (Tharakaraman et al., 2018) (that will be referred to as CHM paper).

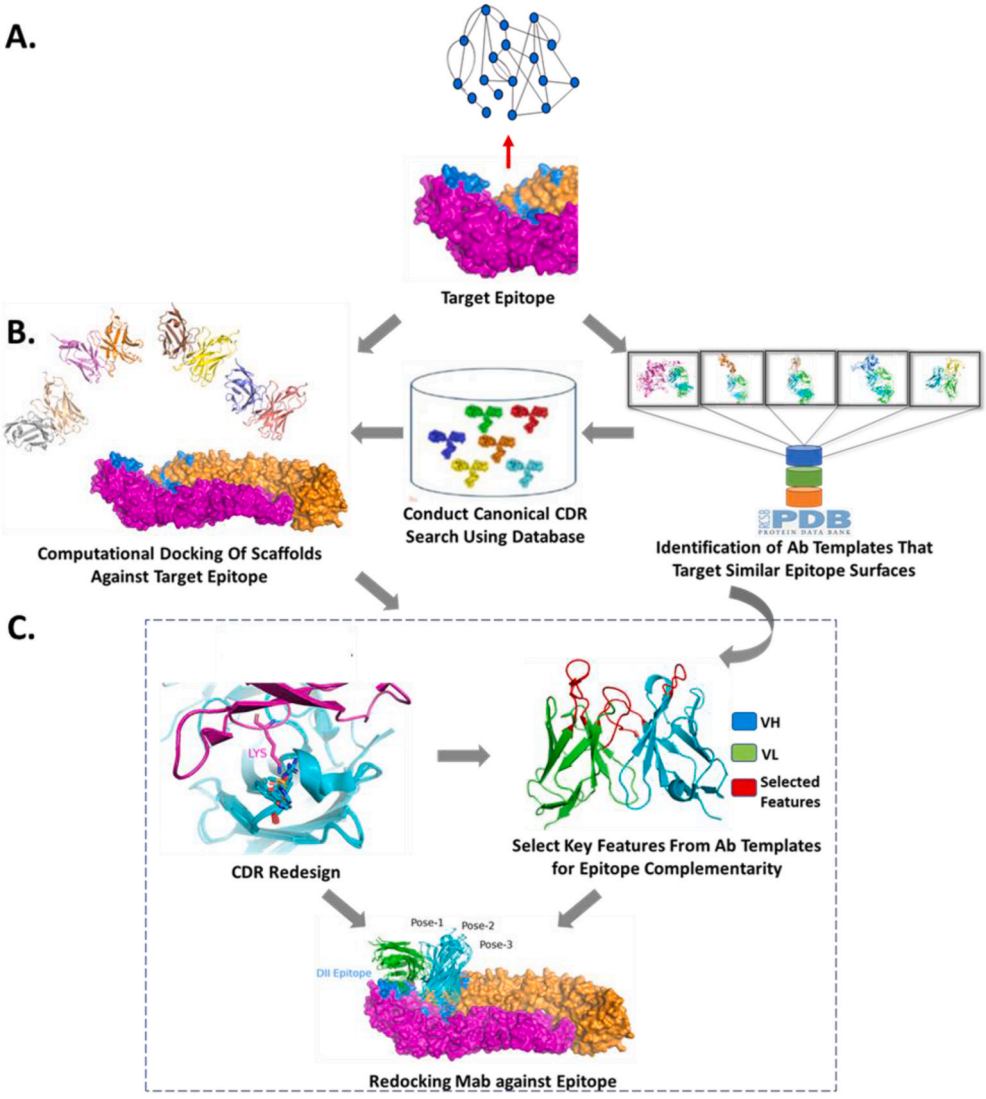

Fig. 1. Schematic illustration of the antibody engineering platform. (A) Epitope identification, (B) computational docking to identify antibody scaffolds with (shape) complementary binding modes, and (C) Iterative design of selected scaffolds by CDR redesign, feature sampling and redocking.

Using engineering of ZAb_FLEP as a case study, we describe herein, the salient features of this antibody-engineering platform. Importantly, we demonstrate with a set of test antibodies derived from different FR-CDR combinations, that despite sharing high overall sequence similarity, the test antibodies yielded diverse (and unexpected from a sequence similarity-based perspective) functional readouts. Therefore, the antibody engineering platform captures key structural nuances of FR-CDR relationships.

2. Results

2.1. The predicted FLEP epitope on zika virus recognized by ZAb_FLEP is distinct from the EDEI epitope recognized by other antibodies

The implementation of the antibody engineering platform starts with defining the target epitope surface (Fig. 1). In the case of engineering an anti-Zika virus (ZIKV) antibody, defining the epitope surface required generating a model of the E-protein capturing the entire quaternary assembly of Dengue and Zika viruses to understand the differences in the epitope surfaces targeted by different antibodies. The epitope selection is driven by a heuristic process that incorporates our understanding of antibody structure-functional relationships to capture a neutralizing epitope region (based on overlap with the fusion loop region) that is -(1) networked and (2) accessible. This, in the context of the 3D assembly, is important to permit favorable antibody binding (such as inter-chain locking) required for potent neutralization, and to avoid the risk of antibody dependent enhancement (ADE). The target epitope that was identified, which we have termed epitope surface proximal to the fusion loop ('FLEP'), contained the largest quantity of highly networked residues and had the largest median solvent-accessible surface area of all known ZIKV antibodies (Table 1). The average network score of residues in the FLEP epitope was more than 25% higher when compared to the average network score of the residues in the E-dimer epitope 1 (EDEI) epitope targeted by other antibodies such as the C8 antibody (Barba-Spaeth et al., 2016) (Table 1). Therefore, the residues in this epitope collectively are less likely to mutate when compared to residues in the EDEI epitope. While thirteen out of the twenty-one (62%) predicted FLEP epitope residues overlap with the C8 epitope (Barba-Spaeth et al., 2016) (Table 1), the remaining 8 residues are unique to FLEP, half of which (329, 369, 370, 371) are located in the DIII domain. In the context of a 3D structure, when compared to the EDEI epitope, the defined FLEP epitope involves more residues from the DIII domain of the non-fusion loop bearing E-chain.

Therefore, the FLEP epitope surface targeted by ZAb_FLEP is different from the EDEI epitope targeted by antibodies such as C8 and C10 on the E-protein assembly of ZIKV. This was recently validated by the 4.1 A° cryo-electron microscopy structure of the complex between the Zika virion and Fab ZAb_FLEP (Tyagi et al., 2020). By comparing the structure with previously published co-crystal structure of Fab C8 – E dimer (ZIKV) complex (Barba-Spaeth et al., 2016), the authors determined that Fab C8 binds a larger epitope surface area than ZAb_FLEP. Further, they identified residues that are unique to the ZAb_FLEP epitope, notably in the DIII domain of an E protein (e.g. N371). These findings are consistent with the predictions of the computational model that identified the FLEP epitope and demonstrate that the FLEP and EDEI epitopes are distinct.

2.2. Engineering ZAb_FLEP antibody

Having identified the FLEP epitope surface on the quaternary E-protein assembly of ZIKV, the next step involved engineering an antibody that could target this surface with the eventual goal of developing this antibody into a therapeutic agent against ZIKV in a clinical setting. Therefore, the key target attributes for engineering were high neutralization potency via binding to the FLEP of different ZIKV strains, and favorable developability metrics - good protein expression, solubility, minimal T-cell epitopes, and reduced potential for off-target binding. The engineering of ZAb_FLEP (described in detail in the Methods section) started with scaffold selection. This process resulted in a starting scaffold with the best shape complementarity to the FLEP epitope, which comprised of an unnatural combination of a heavy chain (VH) of antibody AL-57 targeting human integrin LFA-1 (obtained from PDB: 3HI5 chain H) (Zhang et al., 2009) and a light chain (VL) of anti-CMV antibody (obtained from PDB: 3EYF chain A) (Thomson et al., 2008) (Supplementary Table 1). Owing to the unnatural combination of the heavy and light chains in the scaffold, additional mutations including W35H, Y50A in VH and E1D, L4M, T10S and H38Q in VL were engineered to stabilize the VH/VL interface.

Due to its best shape complementarity with the FLEP epitope, this starting scaffold already possessed some CDR features (such as loop length and composition) that were optimal for binding to the epitope as evaluated by the AIF score and network properties. The next step of paratope engineering began with the CDRs in the starting scaffold and

Table 1
Epitope composition and their properties across the 2-fold interface. Residues common to ZAb_FLEP and C8 epitopes are colored in green whereas residues unique to ZAb_FLEP and C8 epitopes are colored in cyan and orange, respectively. The normalized network score and solvent accessible surface area (SASA) were computed from the E-chain proximal to the 2-fold interface in the asymmetric unit. The normalized network scores for ZAb_FLEP and C8 epitopes are 0.196 & 0.143, respectively, whereas the observed SASA are 56.943 Sq. A (ZAb_FLEP) and 48.278 Sq. A (C8), respectively.

Residue	Amino acid	2-fold normalized network score	2-fold SASA
2	ARG	0.24	32.84
48	THR	0.24	0
67	ASP	0.22	52.09
68	MET	0.06	134.9
69	ALA	0.03	52.56
70	SER	0.07	58.9
71	ASP	0.1	68.35
72	SER	0.09	16.26
73	ARG	0.24	35.65
74	CYS	0.07	23.06
76	THR	0.08	89.32
77	GLN	0.17	31.92
83	ASP	0.12	109.6
97	VAL	0.15	15.53
98	ASP	0.08	31.45
99	ARG	0.21	32.06
101	TRP	0.52	16.33
102	GLY	0.01	42.15
103	ASN	0.09	57.85
104	GLY	0	61.72
105	CYS	0.07	20.89
106	GLY	0.01	17.6
113	LEU	0.2	3.34
251	LYS	0.16	82.97
252	ARG	0.15	105
252	ARG	0.15	105
253	GLN	0.23	19.14
283	ARG	0.21	77.44
315	THR	0.14	30.29
316	LYS	0.26	90.68
329	GLU	0.39	11.23
331	GLN	0.17	55.21
369	THR	0.1	73.02
370	GLU	0.07	110.5
371	ASN	0.12	87.3
373	LYS	0.23	57.19

going through the selection of paratope features from other antibody templates that are known to engage homologous epitope surfaces of related or unrelated antigens (Supplementary Table 2). The complementary determining paratope features from multiple antibody templates including 4G2, C8, C10, A11 (anti-DENV), PGT124 (anti-HIV) and Fab-8-1 (anti-TDRD3) were screened *in silico* for complementarity with the FLEP epitope, from which C8, C10, A11 emerged on top owing to the significant structural homology in the fusion loop region between DENV and ZIKV (as described in Methods section). The assembly of parts was guided by a starting model of antigen-antibody interaction and the AIF metric of each CDR (from scaffold or templates) with the target FLEP epitope. As an example, Supplementary Table 2 shows that the HCDR-1 from the unnatural starting scaffold and HCDR-3 from C8 had the best AIF scores for optimal engagement with the FLEP epitope in the starting model.

The paratope engineering process involved assembly and modifications of both FRs and CDRs to enable binding to the FLEP epitope on ZIKV. The FRs are important for (1) the positioning of the antibody against the target epitope and (2) configuring the CDRs to achieve desired binding affinity to the FLEP epitope. Five designs that met the criteria for paratope engineering (based on AIF scores and network properties), were tested experimentally for expression, yield, binding affinity, and neutralization (Supplementary Table 3). Two of the designed constructs showed poor expression, while one of them showed poor binding to ZIKV and DENV. For one of the constructs, the optimization of the paratope resulted in a rare amino acid substitution that negatively impacted developability. The only construct that cleared all the key protein filters including expression, binding affinity, neutralization potency and developability was subsequently referred to as ZAb_FLEP.

ZAb_FLEP engineering therefore started from the aforementioned unnatural starting scaffold combination, with starting scaffold FR as well as selected CDR features coming from C8 (HCDR2, HCDR3, LCDR1, LCDR3), an antibody that was isolated from plasma blasts of patients infected with Dengue virus (DENV) (Dejnirattisai et al., 2015) (Fig. 2).

2.3. Key features of the antibody engineering platform

The key features of the platform can be elaborated by comparing the distinct attributes of ZAb_FLEP with those of the C8 template from which select CDR features were derived for the engineering of ZAb_FLEP. A detailed comparison at the sequence level of FR and CDR regions of ZAb_FLEP, C8 and the starting heavy and light chain scaffold of ZAb_FLEP is shown in Fig. 2. It is evident from this comparison that the FR of ZAb_FLEP is like that of the unnatural starting scaffold and was not obtained by making random mutations in the FR of C8. Several FR mutations were engineered in ZAb_FLEP to improve the network of VH/VL or FR-CDR or EPCN to improve target binding (see Methods). For example, introducing amino acid changes to Ser or Tyr in the CDRs (Fig. 2) were design choices made based on the abundance of these residues in naturally occurring antibodies' CDR loops, as well as their enhanced ability to mediate antigen recognition (Birtalan et al., 2008).

The key differences in the FRs and CDRs between ZAb_FLEP and C8 are also reflected in the functional differences between these antibodies in their neutralization profile of DENVs and ZIKVs. ZAb_FLEP binds and neutralizes ZIKV from all three lineages tested (Tharakaraman et al., 2018). The neutralization of DENV serotypes by ZAb_FLEP is poor when compared to their potent neutralization by the C8 antibody (Table 1 in CHM paper (Tharakaraman et al., 2018)).

To further demonstrate the importance of the relationship between FRs and CDRs in the assembly and engineering of the relevant parts to generate ZAb_FLEP, a set of control and test designs were generated. The first test antibody (*Test A*) was obtained by assembling CDR loops of C8 (defined using Kabat notation) and a randomly chosen FR (from Herceptin antibody). The second test antibody (*Test B*) was generated by assembling the CDR loops of ZAb_FLEP on the FR of C8. The third test antibody (*Test C*) was generated by assembling the CDR loops of C8 on the FR of the starting scaffolds (3HI5, 3EYF) of ZAb_FLEP, which did not have the optimized network of interactions at the VH/VL interface in the framework or framework-CDR interface to support CDR loops.

The test antibodies along with the control antibodies (ZAb_FLEP and C8) were analyzed for their neutralization potency against representative strains of DENV3 serotype and ZIKV (Table 2). Consistent with earlier publications, C8 showed potent neutralization of both DENV and ZIKV while the neutralization profile of ZAb_FLEP against ZIKV and DENV was substantially different. Despite possessing all the six C8 CDR loops, *Test A* did not possess activity against DENV or ZIKV, indicating that possessing 100% identical CDR loops does not guarantee functional activity. On the other hand, *Test B* that possessed CDRs of ZAb_FLEP showed a neutralization profile for DENV and ZIKV that was like the C8 antibody indicating that the epitope-binding properties of ZAb_FLEP is in turn governed by factors that go beyond the CDRs and require the

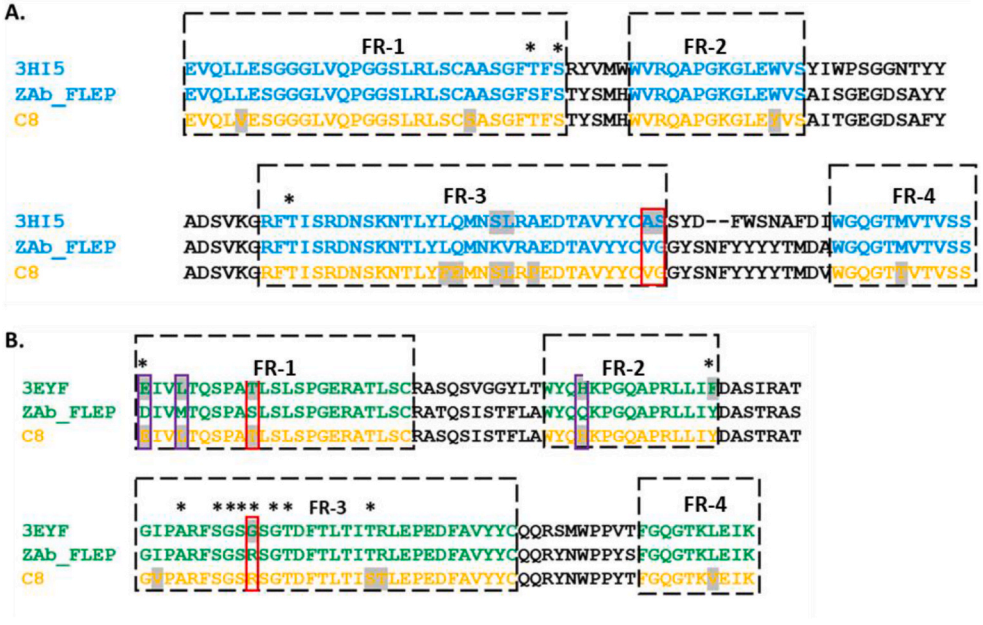

Fig. 2. Starting scaffold for ZAb_FLEP and FR identity to C8. Shown above is an alignment between the VH (A) and VL (B) of the starting scaffolds, ZAb_FLEP, and C8. FR regions (FR1-4) are indicated by dotted boxes. The FR residues of the VH and VL of the starting scaffolds and ZAb_FLEP are colored in blue and green, respectively. The VH and VL FR residues of C8 are colored in orange. CDR residues (defined based on Kabat definition) are uncolored. Amino acids in **FR**s of starting scaffolds and C8 that are different in ZAb_FLEP are highlighted by grey background. Mutations made to FR to optimize VH:VL interface and associated networks are boxed in purple, whereas mutations made to FR to optimize the FR-CDR contacts and associated networks are in red. FR residues that make contact with the FLEP surface of ZIKV are marked with an asterisk above the column. Note that the FRs of ZAb_FLEP are more homologous to that of the starting scaffolds than C8.

Table 2
In vitro neutralization characteristics of test and control mAbs.

	MAb	VH		VL		DENV[a] (EC_{50})	ZIKV ($PRNT_{50}$)	
		FR	CDR	FR	CDR		SG 2016/1	PF13
Test mAbs	Test A	Herceptin Ig	C8	Herceptin Ig	C8	>20	>20	>20
	Test B	C8	Zab_FLEP	C8	Zab_FLEP	0.17	0.01	0.032
	Test C	3HI5	C8	3EYF	C8	>20	>20	>20
Control mAbs	C8	C8	C8	C8	C8	0.24	0.01	0.028
	ZAb_FLEP	ZAb_FLEP	ZAb_FLEP	ZAb_FLEP	ZAb_FLEP	8.08	3.01	0.798

[a] From the CHM paper, it is observed that ZAb_FLEP showed poorest neutralization of DENV serotypes 3 and 4 consistent with its specificity towards ZIKV, on the other hand, C8 showed potent neutralization against all four DENV serotypes. Therefore, to illustrate the impact of the parts assembly on the neutralization of the Test antibodies relative to the control antibodies, DENV serotype 3 was chosen as a representative DENV virus for neutralization.

optimized FR regions of the starting scaffold. Despite having all the C8 CDR loops, *Test C* showed poor to no neutralizing activity against both DENV and ZIKV, indicating the importance of additional FR mutations that were introduced into the starting scaffold while assembling the appropriate parts for ZAb_FLEP. An alignment of the test antibody VH and VL sequences is shown in Fig. 3.

The structure-function relationships of the three test antibodies also emphasize the fact that amino acid substitutions in the framework or VH/VL interface or epitope paratope interface substantially impact the inter-residue interaction network (Fig. 4), and hence impact the functional attributes of the antibody. Also, comparison of the sequences of the various test and control antibodies reveals a high sequence homology (Table 3) of the VH and VL regions despite being functionally distinct. In fact, *Test C* shares greater sequence identity with C8 (93% in VH and 94% in VL) than ZAb_FLEP (89% in VH and 91% in VL). The functional behavior of Test C therefore indicates that 'sequence homology' in the antibody context does not fully explain the observed structure-function relationships. As such, generation of ZAb_FLEP-like antibody via random mutations on C8 based on the sequence homology would be an inefficient, tedious, and extremely unpredictable process. The test antibodies clearly demonstrate the significance of the mutations introduced to optimize key network properties of the FR of the starting scaffold and CDRs.

Analysis of developability characteristics indicated that ZAb_FLEP had fewer predicted immunogenic T-cell epitopes compared to C8, owing to differences in the FR regions (Table 4). ZAb_FLEP also has a lower charge asymmetry than C8 (−3 for ZAb_FLEP vs. −6.3 for C8), a property inherited from the starting scaffold (3HI5:H/3EYF:A). Asymmetry in the net heavy- and light-chain surface charges is correlated with self-association and viscosity at high concentrations (Sharma et al., 2014).

3. Discussion

The antibody engineering platform described in this case study is distinct from other antibody design and engineering approaches, which fall into two categories (1) redesign of existing antibody (e.g., affinity maturation): and (2) ab initio design. Redesign of an antibody starts with the co-crystal structure or homology model of antigen-antibody interaction and tweaks the paratope residues for optimal contacts, without altering the framework residues. Several single mutations (tens to hundreds) are first screened to determine changes in binding affinity/specificity. Subsequently, the promising single mutations are combined in various permutations to determine mutants that lead to the largest impact on affinity/specificity (Clark et al., 2006; Farady et al., 2009; Marvin and Lowman, 2003; Tharakaraman et al., 2013). On the other hand, the ab initio design efforts are aimed at computationally and experimentally screening dozens of VH/VL designs including de novo sampling of CDRs to bind to a target antigen or a defined epitope surface (Adolf-Bryfogle et al., 2018; Baran et al., 2017; Entzminger et al., 2017; Lapidoth et al., 2015; Li et al., 2014). Contrasting with these two approaches, our antibody engineering platform substantially reduces the size of the search and design space. This is achieved by combining pre-defined complementary binding fragments (CDR and/or framework) from antibody structures that target similar epitopes onto corresponding segments of the chosen antibody scaffolds. Subsequently specific mutations in framework and/or CDR are engineered to enhance contact network both within the VH/VL domain and at the

```
Test A    EVQLVESGGGLVQPGGSLRLSCAASGFNIKTYSMHWVRQAPGKGLEWVAAITGEGDSAFY
Test B    EVQLVESGGGLVQPGGSLRLSCSASGFTFSTYSMHWVRQAPGKGLEYVSAISGEGDSAYY
Test C    EVQLLESGGGLVQPGGSLRLSCAASGFTFSTYSMHWVRQAPGKGLEWVSAITGEGDSAFY

Test A    ADSVKGRFTISADTSKNTAYLQMNSLRAEDTAVYYCSRGYSNFYYYYTMDVWGQGTLVTV
Test B    ADSVKGRFTISRDNSKNTLYFEMNSLRPEDTAVYYCVGGYSNFYYYYTMDAWGQGTTVTV
Test C    ADSVKGRFTISRDNSKNTLYLQMNSLRAEDTAVYYCASGYSNFYYYYTMDVWGQGTMVTV

Test A    SS
Test B    SS
Test C    SS

Test A    DIQMTQSPSSLSASVGDRVTITCRASQSISTFLAWYQQKPGKAPKLLIYDASTRATGVPS
Test B    EIVLTQSPATLSLSPGERATLSCRATQSISTFLAWYQHKPGQAPRLLIYDASTRASGVPA
Test C    EIVLTQSPATLSLSPGERATLSCRASQSISTFLAWYQHKPGQAPRLLIFDASTRATGIPA

Test A    RFSGSRSGTDFTLTISSLQPEDFATYYCQQRYNWPPYTFGQGTKVEIK
Test B    RFSGSRSGTDFTLTISTLEPEDFAVYYCQQRYNWPPYSFGQGTKVEIK
Test C    RFSGSGSGTDFTLTITRLEPEDFAVYYCQQRYNWPPYTFGQGTKLEIK
```

Fig. 3. Alignment of VH and VL sequences of test mAbs. CDR regions defined according to Kabat definition are highlighted in grey boxes. Amino acids different from the VH and VL of C8 are marked in red.

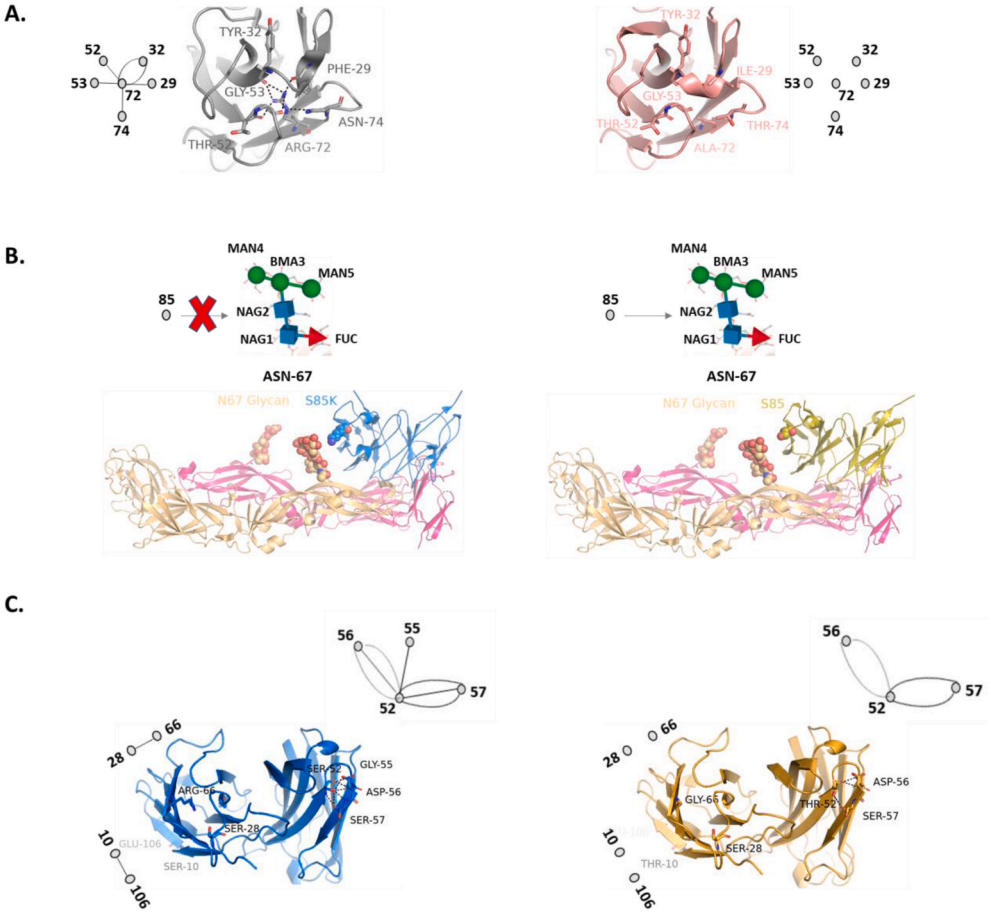

Fig. 4. Illustration of function-altering polar interatomic networks that are absent in the test designs. A. polar interatomic networks formed by the FR residue VH-Arg 72 to support the conformation of H-CDR1 (VH-Phe 29, VH-Tyr32) and H-CDR2 (Thr52, Gly 53) of C8 (*left*) are absent in Test A (*right*) due to the Arg72Ala mutation. B. the potential specificity governing VH-S85K mutation in ZAb_FLEP (*left*) that causes steric clashes with N67 glycan is absent in Test B (*right*). C. interatomic networks formed by the FR residues VL-Arg 66, VL-Ser 10 to support the conformations of LCDR1 (VL-Ser 28) and LCDR3 (VL-Glu 106) of ZAb_FLEP (*left*) are absent in Test C (*right*) due to Arg66Gly and Ser10Thr mutations. Changes to the interatomic network brought about by the conservative CDR substitution VH-Ser52Thr are also depicted. The VH-Ser 52 network in ZAb_FLEP includes residues VH-Gly 55, Asp56 and Ser57 whereas the counterpart network in test mAb C includes just Asp56 and Ser57. The 2D network diagram is shown adjacent to the residue positions contributing to that network in each figure. The circular nodes represent amino acid positions and edges connectivity to other nodes.

Table 3
Sequence identity of the VH and VL components of designed mAbs to C8. Values inside the brackets represent sequence similarity, which takes into consideration conservative substitutions.

	VH	HCDR1	HCDR2	HCDR3	VL	LCDR1	LCDR2	LCDR3
ZAb_FLEP	89.34 (95.08)	100 (100)	88.2 (100)	92.3 (100)	90.65 (98.13)	90.9 (100)	85.71 (100)	90 (100)
Test A	87.7 (90.98)	100 (100)	100 (100)	100 (100)	84.11 (92.52)	100 (100)	100 (100)	100 (100)
Test B	97.54 (100)	100 (100)	88.2 (100)	92.3 (100)	97.2 (100)	90.9 (100)	85.71 (100)	90 (100)
Test C	92.62 (95.08)	100 (100)	100 (100)	100 (100)	94.39 (98.13)	100 (100)	100 (100)	100 (100)

Table 4
In silico immunogenicity assessment of mAbs: putative T-cell epitopes predicted by NetMHCIIpan server (Andreatta et al., 2015). ZAb_FLEP has more favorable profile in terms of T-cell epitopes from a developability standpoint. C8 VL has additional T-Cell epitopes (residues 73–82 and 75–84) that are not present in ZAb_FLEP VL. A peptide is ranked as a strong binder if its predicted affinity is among the top 1% scores of some 200,000 random natural peptides of the same length for the specified allele.

Chain	Predicted T-cell Epitope Peptide Cores
ZAb_FLEP VH	None
ZAb_FLEP VL	47–56
C8 VH	None
C8 VL	[47–56], **[73–82]**, **[75–84]**

epitope-paratope interface. The success of our platform relies on the availability of known sequence and structure information of antibody-antigen complexes which provide starting templates for the search, assembly, and engineering of the antibody parts to generate an antibody with the desired distinct functional properties. The data shown here on the test and control antibodies also illustrate one of the key features of the antibody-engineering platform, optimization of network properties to stabilize FR and CDR parts from other antibodies to assemble and engineer ZAb_FLEP.

The functional consequences of sequence changes at the protein-protein interfaces (or even outside the interface viz., long-range interaction) are well known (Clark et al., 2006; Marvin and Lowman, 2003; Robinson et al., 2015). In the context of the test antibody designs, even a conservative substitution within a CDR loop (VH-Ser52Thr) can lead to drastic changes in the interatomic interactions with the adjacent residues, with potential to impact epitope-paratope contacts (Fig. 4C). The network approach employed in our antibody-engineering platform is able to capture the impact of amino acid substitutions in the FR and CDRs on antigen binding in the context of its structural environment that goes beyond the traditional view that conservative substitutions are less likely to impact function than non-conservative substitutions.

The importance of the framework in optimizing stability and antibody affinity leading to affinity maturation process through indirect ways has been described by many studies (Fukunaga et al., 2018; Ovchinnikov et al., 2018; Zhou et al., 2020). Warszawski et al. showed the affinity of an anti-lysozyme could be improved by ten-fold without modifying the CDR loops by simply introducing changes in the interface

between the heavy and light chains alone (Warszawski et al., 2019). Additionally, the solvent-exposed 'DE' loop of the variable domain fragment considered to be part of the framework is known to affect the conformations of CDR1 and CDR2, and hence the antibody activity (Chothia and Lesk, 1987; Foote and Winter 1992; Lehmann et al., 2015; Tramontano et al., 1990).

Typical computational approaches go through an extensive screening, often evaluating several hundred designs (Baran et al., 2017). Notably, this view of antibody development has guided the misconceptions expressed in a recent article (Vasquez et al., 2019), about origins of ZAb_FLEP – suggesting that it was derived from antibody C8 through non-conservative amino acid substitutions. On the contrary, our antibody engineering platform comprises of a selective process that combines parts of antibodies such as FRs from selected scaffolds and CDRs from other antibodies that recognize parts of the target epitope surface, which are then further engineered to optimize various contact network properties. The methods employed for the paratope engineering of ZAb_FLEP, namely "antibody interface fitness" (AIF) and "multivariate logistic regression" (MLR) (Tharakaraman et al., 2013), were refined through a detailed analysis of antigen-antibody co-crystals from the Protein Data Bank (PDB). Furthermore, given that amino acid network is one of the important properties that is being optimized, if a combination of the engineered scaffold and CDRs with optimal network passes the scoring metrices, it is directly taken for experimental testing for the desired functional properties. Therefore, convergence to a desired solution can occur rapidly, leveraging a highly variable design space based on the specific interaction network of antigen-antibody systems under consideration.

The initial shape complementarity from the starting antibody-antigen structural model and the selection of appropriate template antibody structures governs the choice of the appropriate antibody CDR fragments based on their AIF scores with the epitope surface (Supplementary Table 2). Therefore, if the starting model of the docked antibody-epitope complex was different, or if C8 was not a part of the structural (template) database, then the selection of HCDR-3 would have been derived from other antibody templates, which may or may not have the best AIF score with the FLEP epitope. This then would have required additional CDR/FW mutations for optimization of the AIF and additional experimental iterations to converge on a solution that is different from ZAb_FLEP. Furthermore, the platform's utility is towards targeting epitope surfaces that are homologous to those found in one or more natural antigen-antibody interfaces (to enable template selection), as was the case for ZAb_FLEP. This allowed for the generation of an antibody-based solution in a rapid timeframe to address the ZIKV public health crisis in Singapore in 2016 (Businessinsider, 2018).

Using known information on antibody-antigen complexes and searching a space of antibody sequences that was available at that time enabled engineering of ZAb_FLEP. Since the time ZAb_FLEP was engineered, the sequence and structural information pertaining to antibodies and antibody-antigen interactions in public repositories have dramatically increased owing to human B-cell panning studies and next generation sequencing methodologies. Therefore, the antibody-engineering platform can now be substantially expanded by mining features related to fourteen discrete building blocks (8 FR fragments and 6 CDR loops) from these vast sequence and structural antibody databases. In fact, such approaches are being pursued by others and us (Liu et al., 2019) to engineer antibodies with distinct properties to target specific epitope surfaces. Indeed, using this platform we rapidly developed a mAb against Yellow Fever in 7 months towards filing an Investigational New Drug (IND) application and subsequently successfully completed both a Phase 1a and 1b clinical studies (Low et al., 2020). In addition, we were able to employ this platform to develop a mAb against SARS-CoV-2, file an IND, and successfully complete a Phase 1a clinical study within 6 months with support from the whole Government of Singapore (Business Wire, Dec 2020). Given the strong potential for clinical impact by these therapeutics, it is our view that such efforts should be received with an open mind by the antibody engineering community, alongside other approaches that creatively sample the antibody design space, especially in the context of the rapidly expanding knowledge of the sequence and structural space of human antibodies and their antigens.

4. Methods

4.1. Engineering ZAb_FLEP

The antibody-engineering platform (see http://sasilab.mit.edu/3dmabdesign-platform/for a simple animation) comprises of two components: (1) scaffold selection and (2) paratope engineering. The scaffold selection starts from identifying appropriate antibody templates from more than 450 antigen-antibody co-crystal structures in the protein databank (www.rcsb.org). The selection criteria include CDRs that engage with the epitope surface defined based on sequence homology to FLEP epitope surface and RMSD threshold from structural superposition of lower than 1.5 Å. The FLEP epitope is a highly discontinuous/quaternary epitope. To simplify the search process, we considered the epitope region to be a fragment of the E-DII domain (residues A63-S122, PDB: 5IRE numbering followed). Superimposing the published DENV antibody complexes (C8 - 4UTA, C10 - 4UT9, A11 - 4UTB) onto the ZIKV E-DII fragment established C8, C10, A11 as promising templates based on structural homology (RMSD) between the E-DII fragments. Although 4G2 does not have a crystal structure, it is known to target the fusion loop peptide of DENV serotypes 1-4, which qualified the antibody as a potential template. The anti-HIV antibody PGT124 targets a glycopeptide epitope on gp120 (PDB: 4R26). The potential for it to recognize a region harboring the conserved N-glycosylation (N154) located near the fusion peptide of E-protein was evaluated by structural modeling. Using PyMOL, we superimposed PGT124-HIV oligosaccharide from PDB: 4R2G manually on the E dimer of ZIKV keeping the GlcNAc subunit as the point of alignment. This revealed that PGT124 can recognize the epitope through the oligosaccharide unit without steric issues albeit the orientation of the Fab will prevent it from engaging with the peptide backbone.

To further broaden the search for templates, we employed PDBePISA (https://www.ebi.ac.uk/pdbe/pisa/) to identify other candidates. PDBePISA returns structurally similar interfaces given an input protein-protein complex and user-defined similarity thresholds for the chains involved in the interface. Because of the overlap between EDE1/EDE2 and FLEP epitopes and since our epitope analyses with Dengue antibodies indicated that inter-chain locking potential, network scores and epitope accessibility correlated most with the $PRNT_{50}$ values, we employed EDE mAb complex (such as C8, C10, A11 or B7) wherein the E protein was truncated to only include the fragment (residues A63-S122) as input to PDBePISA. We employed similarity thresholds: VH: 40%, DII: 50% to determine structurally homologous interfaces. Note that the relatively higher epitope similarity threshold is meant to capture homologous chains in PDB. After removing redundant entries and entries not containing a Fab or Fv subunit, the resulting list potential antibody templates including anti-Gonadotropin alpha subunit (1QFW), anti-TDRD3 FAB (3PNW), anti-HIV (3LH2), which were highlighted as representative antibodies in Fig. 1B of the original CHM paper. We note that the results are not overly sensitive to the input parameters – as a matter of fact, similar results can be obtained by switching the Fab, fragment type (DENV or ZIKV), fragment length (e.g. employing a smaller fragment ALA63-LYS122 does not exclude the aforementioned templates but affected their ranking within the top 200 hits) and Fab-DII orientation (as long as the Fab (i) does not cause steric clashes with any E-chain when placed in the context of virion assembly and (ii) engages a portion of the FLEP epitope residues embedded in the DII fragment, i.e., 67ASP, 73ARG, 76THR, 83ASP, 97VAL, 98ASP, 99ARG, 101TRP).

These template antibodies were used to expand the search space to include naturally occurring antibody sequences of 8718 human VH, 8513 human VK and 6779 human VL sequences from the NCBI GenBank

database. Considering only those that had similar canonical CDRs (as those of the chosen templates) narrowed the antibody search space. The set of canonical CDRs used in the search process include (1) L1:2/11 A, L2:1/7 A, L3:1/9 A, H1:1/10 A, H2:2/10 A), (2) (L1:2/11 A, L2:1/7 A, L3: N/A, H1:1/10 A, H2:1/9 A), and (3) (L1:2/11 A, L2:1/7 A, L3:5/11 A, H1:3/12 A, H2:2/10 A). Additionally, the antibodies that matched one of these classes needed to also meet an initial set of developability criteria such as abundance of predicted T-cell epitopes. Binding sites of MHC II alleles were predicted using NetMHCIIpan server whereby a peptide is ranked as a strong binder if its predicted affinity is among the top 1% scores of some 200,000 random natural peptides of the same length for the specified allele. From the set of scaffolds that met these criteria, homology based structural models of the VH and VL (for those scaffolds which do not have an X-ray crystal structure) were constructed. From these, representative antibody scaffolds (with natural and unnatural pairing) are employed for computational docking. The structures or structural models of the selected scaffolds are then docked using ZDOCK software (http://zdock.umassmed.edu/) using default docking parameters including the appropriate force fields and using additional constraints from epitope-paratope engagement. As stated in the CHM paper, E-protein residues that have accessible surface area >20% and network score >0.25 were selected as constraints. On the paratope front, residue positions that are accessible and more likely to participate in the antigen-antibody interface (e.g. Tyr, Trp) were chosen. HCDR3, LCDR1, LCDR3 frequently contribute to the antigen-antibody interface and H_99, L_32, L_94 are solvent exposed in most antibody structures. The docked poses are ranked based on shape complementarity and knowledge of known poses of antibody engagement with regions on the FLEP gathered from analysis of overlapping epitope regions from other known antibody-antigen complexes. An antibody scaffold containing the variable heavy chain of AL-57 antibody targeting human integrin LFA-1 and the light chain of an anti-CMV antibody (both of which had solved X-ray crystal structures) satisfied the shape complementarity (Sc > 0.60–0.65) and hence was taken forward. We note that we did not carry out exhaustive docking analyses of all the theoretically possible Fvs that could be built from the available VH X VL combinations. Indeed, such a search could potential yield other promising starting scaffolds but optimizing developability and shape complementarity were not the goal of the process, although that could be done, in practice, by executing multiple docking runs simultaneously using parallel computing to generate a library of designs. The top ranked scaffold is selected for the second component of paratope engineering (see Supplementary Figure 1 for an overview of the scaffold selection process and Supplementary Table 1 for a representative set of scaffolds and their properties).

From the initial model of the antigen-antibody interaction, the contributions of the CDR residues in the starting scaffold's binding to the FLEP epitope were evaluated *in silico* using AIF one at a time, beginning with the residue that is most buried and proceeding all the way to the residue that is least buried (Tharakaraman et al., 2018). Some of the CDR features including loop length and AIF scores of the starting scaffold were already optimal to engage with the FLEP epitope (e.g. HCDR1, LCDR2) whereas in the case of HCDR3, these features had to be optimized by sampling other antibody templates (Supplementary Table 2). The selection of the CDR features (loop length and modifications to optimize AIF scores) from other template antibodies showed that some of the residues in the CDR segments from other antibodies provided optimal contact with the FLEP epitope, not all the segments in their entirety are optimal in the context of epitope-paratope interactions. To further optimize the CDRs, multiple CDR loop features were simultaneously selected (including loop lengths and amino acid substitutions) for optimal epitope-paratope interactions, which was evaluated using a combination of AIF scores, binding energy, EPCN and visual inspection. The initial antigen-antibody binding mode selected based on shape complementarity undergoes changes during iterative cycles of redocking with the modified paratope (Fig. 1) and the mutations (or CDR loop features) designed in any given cycle are carried to the next as long as they are not detrimental to the epitope-paratope interface. The paratope engineering process resulted in 5 designs of different CDR features selected on the starting scaffold (Supplementary Table 3). These designs were taken forward for experimental screening to evaluate expression, solubility, binding affinity, and neutralization potency.

4.2. Design of test antibodies

The test antibody designs were generated by grafting the Kabat CDR loops of C8 (Test A, C) or ZAb_FLEP (Test B) onto the framework regions of different antibodies: Herceptin (Test A), C8 (Test B) and 3HI5:H (VH)/3EYF:A (VL) (Test C). Herceptin was chosen as a framework for Test A since there are distinct differences in its canonical CDR structures relative to C8, presenting an interesting example to demonstrate the importance of framework to CDR relationship. For instance, the canonical class of L3 CDR loop is 1/9 A in Herceptin, which is different from that of C8.

4.3. Recombinant expression of monoclonal antibodies

Gblock gene fragments for engineered VH and VL sequences were cloned into pcDNA3.0 plasmid encoding heavy chain and light chain respectively before transfection into ExpiCHO-S cells in 30 mL scale. Antibodies were purified from supernatants on an ÄKTA Avant 150 protein A purification system followed by dialysis to formulate them in PBS and sterile filtered. All purified antibodies were stored at −80 °C for long term storage.

4.4. Neutralization potency testing against ZIKV & DENV3

The neutralization activity was tested by plaque reduction neutralization test (PRNT) for ZIKV and an ELISA based microneutralization assay for DENV3. For the PRNT serially diluted antibody was mixed with an equal volume of individually diluted ZIKV strains (SG 2016/1, PF13 (GenBank: MG827392) or MR766 (GenBank: LC002520)) and incubated for 1 h at 37 °C. The virus-antibody mixture was then applied to BHK21 cell monolayers in 24-well plates and incubated for 1 h at 37 °C. After incubation, the virus-antibody mixture was removed and the cells were overlaid with semi-solid CMC overlay, and incubated for 5 days at 37 °C before the cells were fixed with 10% formalin and stained with 1% crystal violet. Plaques were counted and normalized to the mean of the virus control (no antibody). Plaque counts were plotted against the transformed concentrations of the antibody tested using GraphPad PRISM software and the $PRNT_{50}$ calculated.

For the microneutralization assay, serially diluted antibody was mixed with an equal volume of diluted DENV3 863 DK1 and incubated for 1 h at 37 °C. The virus-antibody mixture was then applied to VERO cell monolayers in 96-well plates and incubated at 37 °C for 5 days. After incubation, the cells are fixed overnight at −20 °C with cold 1:1 methanol-ethanol solution. The next day, mouse antibody, 4G2, followed by detection with a horseradish peroxidase (HRP)-conjugated anti-mouse antibody was used to measure the cell-associated viral antigens. TMB substrate solution was used to detect HRP activity and read at 650 nm using a plate reader. The mean absorbance of the response was calculated by subtracting the mean absorbance of the background signal, which are the wells without virus. These values were subsequently plotted against the transformed concentrations of the antibody using GraphPad PRISM software and the EC_{50} calculated.

Declaration of competing interest

The authors declare the following financial interests/personal relationships which may be considered as potential competing interests: Debbie Ching Ping Lee, Nahdiyah Abdul Ghafar and Yadunanda Budigi are employees of Tychan Pte Ltd.

Acknowledgements

The Authors would like to thank Jannah Dzulkiflie and Jannah Lim from Tychan Pte Ltd for their excellent technical assistance.

Appendix A. Supplementary data

Supplementary data to this article can be found online at https://doi.org/10.1016/j.antiviral.2021.105105.

References

Adolf-Bryfogle, J., Kalyuzhniy, O., Kubitz, M., Weitzner, B.D., Hu, X., Adachi, Y., Schief, W.R., Dunbrack Jr., R.L., 2018. RosettaAntibodyDesign (RAbD): a general framework for computational antibody design. PLoS Comput. Biol. 14, e1006112.

Andreatta, M., Karosiene, E., Rasmussen, M., Stryhn, A., Buus, S., Nielsen, M., 2015. Accurate pan-specific prediction of peptide-MHC class II binding affinity with improved binding core identification. Immunogenetics 67, 641–650.

Baran, D., Pszolla, M.G., Lapidoth, G.D., Norn, C., Dym, O., Unger, T., Albeck, S., Tyka, M.D., Fleishman, S.J., 2017. Principles for computational design of binding antibodies. Proc. Natl. Acad. Sci. U. S. A. 114, 10900–10905.

Barba-Spaeth, G., Dejnirattisai, W., Rouvinski, A., Vaney, M.C., Medits, I., Sharma, A., Simon-Loriere, E., Sakuntabhai, A., Cao-Lormeau, V.M., Haouz, A., England, P., Stiasny, K., Mongkolsapaya, J., Heinz, F.X., Screaton, G.R., Rey, F.A., 2016. Structural basis of potent Zika-dengue virus antibody cross-neutralization. Nature 536, 48–53.

Birtalan, S., Zhang, Y., Fellouse, F.A., Shao, L., Schaefer, G., Sidhu, S.S., 2008. The intrinsic contributions of tyrosine, serine, glycine and arginine to the affinity and specificity of antibodies. J. Mol. Biol. 377, 1518–1528.

Businessinsider, 2018. Tychan successfully completes human safety studies for the first-in-class potent monoclonal antibody against Zika virus. https://markets.businessinsider.com/news/stocks/tychan-successfully-completes-human-safety-studies-for-the-first-in-class-potent-monoclonal-antibody-against-zika-virus-1027665842 (Businessinsider).

BusinessWire, Dec 2020. Tychan to start COVID-19 Phase 3 clinical trial for novel monoclonal antibody TY027. Phase 1 clinical trials demonstrate safety of this novel monoclonal antibody. https://www.businesswire.com/news/home/20201210006232/en/Tychan-to-Start-COVID-19-Phase-3-Clinical-Trial-For-Novel-Monoclonal-Antibody-TY027 (Business Wire).

Chothia, C., Lesk, A.M., 1987. Canonical structures for the hypervariable regions of immunoglobulins. J. Mol. Biol. 196, 901–917.

Clark, L.A., Boriack-Sjodin, P.A., Eldredge, J., Fitch, C., Friedman, B., Hanf, K.J., Jarpe, M., Liparoto, S.F., Li, Y., Lugovskoy, A., Miller, S., Rushe, M., Sherman, W., Simon, K., Van Vlijmen, H., 2006. Affinity enhancement of an in vivo matured therapeutic antibody using structure-based computational design. Protein Sci. 15, 949–960.

Cockburn, J.J., Navarro Sanchez, M.E., Fretes, N., Urvoas, A., Staropoli, I., Kikuti, C.M., Coffey, L.L., Arenzana Seisdedos, F., Bedouelle, H., Rey, F.A., 2012. Mechanism of dengue virus broad cross-neutralization by a monoclonal antibody. Structure 20, 303–314.

Dejnirattisai, W., Wongwiwat, W., Supasa, S., Zhang, X., Dai, X., Rouvinski, A., Jumnainsong, A., Edwards, C., Quyen, N.T.H., Duangchinda, T., Grimes, J.M., Tsai, W.Y., Lai, C.Y., Wang, W.K., Malasit, P., Farrar, J., Simmons, C.P., Zhou, Z.H., Rey, F.A., Mongkolsapaya, J., Screaton, G.R., 2015. A new class of highly potent, broadly neutralizing antibodies isolated from viremic patients infected with dengue virus. Nat. Immunol. 16, 170–177.

Entzminger, K.C., Hyun, J.M., Pantazes, R.J., Patterson-Orazem, A.C., Qerqez, A.N., Frye, Z.P., Hughes, R.A., Ellington, A.D., Lieberman, R.L., Maranas, C.D., Maynard, J.A., 2017. De novo design of antibody complementarity determining regions binding a FLAG tetra-peptide. Sci. Rep. 7, 10295.

Farady, C.J., Sellers, B.D., Jacobson, M.P., Craik, C.S., 2009. Improving the species cross-reactivity of an antibody using computational design. Bioorg. Med. Chem. Lett 19, 3744–3747.

Foote, J., Winter, G., 1992. Antibody framework residues affecting the conformation of the hypervariable loops. J. Mol. Biol. 224, 487–499.

Fukunaga, A., Maeta, S., Reema, B., Nakakido, M., Tsumoto, K., 2018. Improvement of antibody affinity by introduction of basic amino acid residues into the framework region. Biochem Biophys Rep 15, 81–85.

Hu, D., Hu, S., Wan, W., Xu, M., Du, R., Zhao, W., Gao, X., Liu, J., Liu, H., Hong, J., 2015. Effective optimization of antibody affinity by phage display integrated with high-throughput DNA synthesis and sequencing technologies. PloS One 10, e0129125.

Lapidoth, G.D., Baran, D., Pszolla, G.M., Norn, C., Alon, A., Tyka, M.D., Fleishman, S.J., 2015. AbDesign: an algorithm for combinatorial backbone design guided by natural conformations and sequences. Proteins 83, 1385–1406.

Lehmann, A., Wixted, J.H., Shapovalov, M.V., Roder, H., Dunbrack Jr., R.L., Robinson, M.K., 2015. Stability engineering of anti-EGFR scFv antibodies by rational design of a lambda-to-kappa swap of the VL framework using a structure-guided approach. mAbs 7, 1058–1071.

Li, T., Pantazes, R.J., Maranas, C.D., 2014. OptMAVEn–a new framework for the de novo design of antibody variable region models targeting specific antigen epitopes. PloS One 9, e105954.

Lippow, S.M., Wittrup, K.D., Tidor, B., 2007. Computational design of antibody-affinity improvement beyond in vivo maturation. Nat. Biotechnol. 25, 1171–1176.

Liu, Q., Lai, Y.T., Zhang, P., Louder, M.K., Pegu, A., Rawi, R., Asokan, M., Chen, X., Shen, C.H., Chuang, G.Y., Yang, E.S., Miao, H., Wang, Y., Fauci, A.S., Kwong, P.D., Mascola, J.R., Lusso, P., 2019. Improvement of antibody functionality by structure-guided paratope engraftment. Nat. Commun. 10, 721.

Low, J.G., Ng, J.H.J., Ong, E.Z., Kalimuddin, S., Wijaya, L., Chan, Y.F.Z., Ng, D.H.L., Tan, H.C., Baglody, A., Chionh, Y.H., Lee, D.C.P., Budigi, Y., Sasisekharan, R., Ooi, E. E., 2020. Phase 1 trial of a therapeutic anti-yellow fever virus human antibody. N. Engl. J. Med. 383, 452–459.

Lu, R.M., Hwang, Y.C., Liu, I.J., Lee, C.C., Tsai, H.Z., Li, H.J., Wu, H.C., 2020. Development of therapeutic antibodies for the treatment of diseases. J. Biomed. Sci. 27, 1.

Marvin, J.S., Lowman, H.B., 2003. Redesigning an antibody fragment for faster association with its antigen. Biochemistry 42, 7077–7083.

Ovchinnikov, V., Louveau, J.E., Barton, J.P., Karplus, M., Chakraborty, A.K., 2018. Role of framework mutations and antibody flexibility in the evolution of broadly neutralizing antibodies. Elife 7.

Pantazes, R.J., Maranas, C.D., 2010. OptCDR: a general computational method for the design of antibody complementarity determining regions for targeted epitope binding. Protein Eng. Des. Sel. 23, 849–858.

Poosarla, V.G., Li, T., Goh, B.C., Schulten, K., Wood, T.K., Maranas, C.D., 2017. Computational de novo design of antibodies binding to a peptide with high affinity. Biotechnol. Bioeng. 114, 1331–1342.

Robinson, L.N., Tharakaraman, K., Rowley, K.J., Costa, V.V., Chan, K.R., Wong, Y.H., Ong, L.C., Tan, H.C., Koch, T., Cain, D., Kirloskar, R., Viswanathan, K., Liew, C.W., Tissire, H., Ramakrishnan, B., Myette, J.R., Babcock, G.J., Sasisekharan, V., Alonso, S., Chen, J., Lescar, J., Shriver, Z., Ooi, E.E., Sasisekharan, R., 2015. Structure-guided design of an anti-dengue antibody directed to a non-immunodominant epitope. Cell 162, 493–504.

Scheid, J.F., Mouquet, H., Feldhahn, N., Seaman, M.S., Velinzon, K., Pietzsch, J., Ott, R. G., Anthony, R.M., Zebroski, H., Hurley, A., Phogat, A., Chakrabarti, B., Li, Y., Connors, M., Pereyra, F., Walker, B.D., Wardemann, H., Ho, D., Wyatt, R.T., Mascola, J.R., Ravetch, J.V., Nussenzweig, M.C., 2009. Broad diversity of neutralizing antibodies isolated from memory B cells in HIV-infected individuals. Nature 458, 636–640.

Sharma, V.K., Patapoff, T.W., Kabakoff, B., Pai, S., Hilario, E., Zhang, B., Li, C., Borisov, O., Kelley, R.F., Chorny, I., Zhou, J.Z., Dill, K.A., Swartz, T.E., 2014. In silico selection of therapeutic antibodies for development: viscosity, clearance, and chemical stability. Proc. Natl. Acad. Sci. U. S. A. 111, 18601–18606.

Soundararajan, V., Zheng, S., Patel, N., Warnock, K., Raman, R., Wilson, I.A., Raguram, S., Sasisekharan, V., Sasisekharan, R., 2011. Networks link antigenic and receptor-binding sites of influenza hemagglutinin: mechanistic insight into fitter strain propagation. Sci. Rep. 1, 200.

Tharakaraman, K., Robinson, L.N., Hatas, A., Chen, Y.L., Siyue, L., Raguram, S., Sasisekharan, V., Wogan, G.N., Sasisekharan, R., 2013. Redesign of a cross-reactive antibody to dengue virus with broad-spectrum activity and increased in vivo potency. Proc. Natl. Acad. Sci. U. S. A. 110, E1555–E1564.

Tharakaraman, K., Watanabe, S., Chan, K.R., Huan, J., Subramanian, V., Chionh, Y.H., Raguram, A., Quinlan, D., McBee, M., Ong, E.Z., Gan, E.S., Tan, H.C., Tyagi, A., Bhushan, S., Lescar, J., Vasudevan, S.G., Ooi, E.E., Sasisekharan, R., 2018. Rational engineering and characterization of an mAb that neutralizes Zika virus by targeting a mutationally constrained quaternary epitope. Cell Host Microbe 23, 618–627 e616.

Thomson, C.A., Bryson, S., McLean, G.R., Creagh, A.L., Pai, E.F., Schrader, J.W., 2008. Germline V-genes sculpt the binding site of a family of antibodies neutralizing human cytomegalovirus. EMBO J. 27, 2592–2602.

Tramontano, A., Chothia, C., Lesk, A.M., 1990. Framework residue 71 is a major determinant of the position and conformation of the second hypervariable region in the VH domains of immunoglobulins. J. Mol. Biol. 215, 175–182.

Tyagi, A., Ahmed, T., Shi, J., Bhushan, S., 2020. A complex between the Zika virion and the Fab of a broadly cross-reactive neutralizing monoclonal antibody revealed by cryo-EM and single particle analysis at 4.1 A resolution. J. Struct. Biol. X 4, 100028.

Vasquez, M., Krauland, E., Walker, L., Wittrup, D., Gerngross, T., 2019. Connecting the sequence dots: shedding light on the genesis of antibodies reported to be designed in silico. mAbs 11, 803–808.

Viswanathan, K., Shriver, Z., Babcock, G.J., 2015. Amino acid interaction networks provide a new lens for therapeutic antibody discovery and anti-viral drug optimization. Curr Opin Virol 11, 122–129.

Warszawski, S., Borenstein Katz, A., Lipsh, R., Khmelnitsky, L., Ben Nissan, G., Javitt, G., Dym, O., Unger, T., Knop, O., Albeck, S., Diskin, R., Fass, D., Sharon, M., Fleishman, S.J., 2019. Optimizing antibody affinity and stability by the automated design of the variable light-heavy chain interfaces. PLoS Comput. Biol. 15, e1007207.

Zhang, H., Liu, J.H., Yang, W., Springer, T., Shimaoka, M., Wang, J.H., 2009. Structural basis of activation-dependent binding of ligand-mimetic antibody AL-57 to integrin LFA-1. Proc. Natl. Acad. Sci. U. S. A. 106, 18345–18350.

Zhou, J.O., Zaidi, H.A., Ton, T., Fera, D., 2020. The effects of framework mutations at the variable domain interface on antibody affinity maturation in an HIV-1 broadly neutralizing antibody lineage. Front. Immunol. 11, 1529.